Comprehensive Temporal Protein Dynamics during the Diauxic Shift in *Saccharomyces cerevisiae*

J. Patrick Murphy‡, Ekaterina Stepanova‡, Robert A. Everley‡, Joao A. Paulo‡, and Steven P. Gygi‡§

Yeast (*Saccharomyces cerevisiae*) has served as a key model system in biology and as a benchmark for "omics" technology. Although near-complete proteomes of log phase yeast have been measured, protein abundance in yeast is dynamic, particularly during the transition from log to stationary phase. Defining the dynamics of proteomic changes during this transition, termed the diauxic shift, is important to understand the basic biology of proliferative *versus* quiescent cells. Here, we perform temporal quantitative proteomics to fully capture protein induction and repression during the diauxic shift. Accurate and sensitive quantitation at a high temporal resolution and depth of proteome coverage was achieved using TMT10 reagents and LC-MS3 analysis on an Orbitrap Fusion tribrid mass spectrometer deploying synchronous precursor selection. Triplicate experiments were analyzed using the *time-course* R package and a simple template matching strategy was used to reveal groups of proteins with similar temporal patterns of protein induction and repression. Within these groups are functionally distinct types of proteins such as those of glyoxylate metabolism and many proteins of unknown function not previously associated with the diauxic shift (*e.g.* YNR034W-A and FMP16). We also perform a dual time-course experiment to determine Hap2-dependent proteins during the diauxic shift. These data serve as an important basic model for fermentative *versus* respiratory growth of yeast and other eukaryotes and are a benchmark for temporal quantitative proteomics. ***Molecular & Cellular Proteomics 14: 10.1074/mcp.M114.045849, 2454–2465, 2015.***

The yeast proteome serves as a valuable model in systems biology (1) and as such has been used to gauge technological milestones in proteomics. In recent years, the depth of protein identification in logarithmically-growing yeast has expanded to near-comprehensiveness (>4000 identified proteins) (2-3). However, the yeast proteome is dynamic, and understanding regulatory networks requires a comprehensive grasp of the timing of induction or repression of specific sets of proteins. Proteome dynamics in yeast depend largely on substrate availability, the major of which is glucose. The diauxic shift, the transition from log phase growth on glucose to stationary phase upon glucose exhaustion, involves temporal coordination of protein regulation that is still not completely understood. Because log phase yeast resemble fermentative cancer cells, the diauxic shift is also considered important basic model for understanding the requirements of proliferative cell growth. As such, a landmark gene expression study of the diauxic shift at the transcript level (4) has served as an important resource in biology (5). However, despite recent progress, the dynamic nature of the diauxic shift at the proteome level has not been adequately explored. Doing so requires the ability to perform comprehensive quantitative proteomic analysis with a sufficient number of time-points to resolve the timing of protein induction or repression. Although temporal proteomic data changes have recently been reported within both log and stationary phase (6) using six-plex quantitative proteomics with TMT, and during the transition between log and stationary phase using a four-plex Neucode strategy, highly resolved proteomic data able to fully capture protein dynamics between the two states are lacking.

Several recent advances in mass spectrometry and multiplexed quantitative proteomics potentiate accurate measurements of highly resolved time courses at a comprehensive depth of proteome coverage. First, tandem mass tag technology (TMT)[1] has been expanded to compare up to 10 samples simultaneously (TMT10) using isotopologue-containing reporter ions distinguishable by high-resolution mass spectrometry (7). TMT reagents work on the principle of isobaric tagging whereby their addition to a peptide maintains a nominal mass, but cleavable reporter ions are used to compare peptide abundance between samples (8). Second, although

From the ‡Department of Cell Biology, Harvard Medical School, Boston, Massachusetts, 02115

Received October 23, 2014, and in revised form, June 5, 2015
Published, MCP Papers in Press, June 15, 2015, DOI 10.1074/mcp.M114.045849
Author contributions: J.P.M. designed research; J.P.M., E.S., R.A.E., and J.A.P. performed research; J.P.M. contributed new reagents or analytic tools; J.P.M. analyzed data; J.P.M. and S.P.G. wrote the paper.

[1] The abbreviations used are: TMT, tandem mass tag; TMT10, 10 sample TMT; ADH, alcohol dehydrogenase; ALD, aldehyde dehydrogenase.

isobaric reporter ion tagging strategies have been plagued by interference from co-isolated peptides, using MS3 scans for reporter ion quantitation has been shown to ensure quantitative accuracy (9). Third, the MS3 approach has recently been enhanced by techniques to isolate multiple MS2 precursors (SPS) for greater MS3 scan sensitivity (10). These advancements, deployed on the Orbitrap Fusion tribrid mass spectrometer allow high temporal resolution (10 time points), proteomic depth (>4500 proteins), and quantitative accuracy (11). We here aimed to fully capture the intricate temporal proteome dynamics over the full diauxic shift at a comprehensive level using 10-plex TMT and LC-MS3.

The data we present here extend current understanding of protein dynamics during diauxic shift in yeast by virtue of the high temporal resolution and comprehensive depth achieved. Data were collected in triplicate allowing us to assess temporal significance, following which we applied a simple template-profile matching strategy to map the timing of induction or repression of proteins of specific functions in relation to glucose exhaustion. The data set also resolves the timing of the induction of many proteins of unknown function (*e.g.* FMP16, YNR034W-A, and TMA17) as well those not previously associated with the transition to stationary phase (*e.g.* YKL065W-A and PAI3). In an additional, dual time-course experiment, we show both high reproducibility between analyses of different strains and provide a putative list of proteins dependent on the respiratory growth-related transcription factor, Hap2. These include many known Hap2-dependent proteins such as those of glyoxylate metabolism and oxidative phosphorylation as well as several novel Hap2-dependent proteins supporting carnitine metabolism (*e.g.* AGP2). These data serve as a benchmark in temporal quantitative proteomics and are a valuable resource for the biological community in understanding fermentative *versus* respiratory metabolism in eukaryotic cells.

EXPERIMENTAL PROCEDURES

Yeast Culture and Harvest—The yeast strain DBY7286 was obtained from the laboratory of David Botstein, Princeton University (Princeton, NJ) and S288C (WT and ΔHap2) was from the Matα deletion collection (BY4742; Matα, his3Δ, leu2Δ, lys2Δ, ura3Δ) (Open Biosystems, Hunstville, AL). TAP tag strains used in validation experiments or ΔHap2 experiments were either from the TAP tag collection or made as described therein (12). For temporal proteomics experiments, an overnight culture was used to inoculate 1L cultures, in triplicate, at an OD600 nm of 0.1 and cultures were grown at 30 °C with shaking (250 RPM) in yeast peptone dextrose media. The volume harvested for the first time point was 50 ml and subsequent harvest volumes were prorated to contain an equal number of cells based on the OD600 nm. Cells were pelleted at 2500 × *g*, washed once with water and stored at −80 °C.

Protein Extraction, Digest, and TMT Labeling—Cells were lysed in 6 M guanidine-HCl, 50 mM HEPES, pH 8.5, containing Roche complete mini protease inhibitor mixture (2 tablets per 10 ml) (Roche, Madison, WI). Lysis was performed by three cycles of bead beating (45 s per cycle) with 1 min rests on ice between cycles using a BioSpec Mini-Beadbeater. Lysates were cleared by centrifugation at 13,000 × *g* for 5 min. Protein concentrations were determined using a BCA assay (Thermo-Fisher Scientific, Rochford, IL). Cysteine residues in the lysates were reduced using 5 mM dithiothreitol for 40 min at room temperature, then alkylated using 14 mM iodoacetamide for 40 min in the dark at room temperature and quenched using 5 mM dithiothreitol. Aliquots containing 100 μg of protein were diluted to 1.5 M guanidine-HCl, 50 mM HEPES (pH 8.5) and digested for 3 h using endoproteinase Lys-C (Wako, Osaka, Japan) at a ratio of 1:200 Lys-C/protein. Samples were then further diluted to 0.5 M Guanidine-HCl and digested overnight with trypsin (Promega, Madison, WI) at a ratio of 1:50 trypsin/protein. Digested peptides were desalted using 50 mg solid-phase C18 extraction cartridges (Waters, Milford, MA) and lyophilized. Dried peptides were re-suspended in 200 mM HEPES (pH 8.5), 30% acetonitrile and labeled using 10 μl of TMT10 (10-plex) reagents (Thermo-Fisher Scientific, Rochford IL) pre-aliquoted at a concentration of 20 μg/ml in anhydrous acetonitrile. The labeling reaction proceeded for 1 h at room temperature, then was quenched with hydroxylamine (Sigma, St. Louis. MO) at a final concentration of 0.5%. Samples were mixed equally, desalted using a 200 mg solid-phase C18 extraction cartridge (Waters), and lyophilized.

2D-LC-MS3—TMT10-labeled samples were fractionated using high-pH reversed phase chromatography performed with an Agilent 300-Extend, 4.6 mm × 250 mm, 5 μm C18 column (Agilent, Santa Clara, CA). The flow rate was 800 μl/min and a gradient of 5% to 40% acetonitrile (10 mM ammonium formate, pH 8) was applied using an Agilent 1100 pump (Agilent). Beginning at 10 min of peptide elution, fractions were collected every 0.38 min. Every 12th fraction was combined to a single sample creating 12 fractions, which were desalted using homemade stage-tips as previously described (13), and lyophilized. For the 10-plex time point data sets (in biological triplicate) each fraction was analyzed on an Orbitrap Fusion (Thermo Fisher Scientific, San Jose, CA) mass spectrometer. All fractions in the first replicate were also analyzed using an Orbitrap Elite mass spectrometer (Thermo Fisher Scientific). The 10-plex experiment comparing ΔHap2 to WT was analyzed on an Orbitrap Elite mass spectrometer. Chromatography for LC-MS3 analysis on both mass spectrometers was performed using identical chromatography methods applied using a Thermo EASY nLC (Thermo Fisher Scientific, Rockford, IL). Peptides were separated on a 75 μm × 30 cm column packed with 0.5 cm of Magic C4 resin (5 μm, Michrom Bioresources, Auburn, CA) and the remainder of the column with Maccel C18 AQ resin (3 μm, Nest Group, Southborough, MA). Peptides were separated at a flow rate of 300 nL/min using a gradient of 8–26% acetonitrile (0.125% formic acid) over 170 min followed by 10 min at 100% acetonitrile. LC-MS3 analysis on the Elite was performed as previously described (7). Briefly, over a 3 h gradient of peptide elution the 10 most abundant MS1 ions were fragmented and multiple MS2 ions were selected for a specialized MS3 scan where multiple MS2 ions are captured for the MS3 scan (an early version of SPS based on collection of multiple isolation notches). For LC-MS3 analysis on the Fusion, MS1 scans were acquired over an *m/z* range of 400–1400, 120K resolution, AGC target of 2e5, maximum injection time of 100 msec. MS2 scans were acquired on the 10 most-abundant MS1 ions of charge state 2–6 using an isolation window of 0.5 Th, CID activation with a collision energy of 35%, rapid scan rate, AGC target of 4000, dynamic exclusion for 30 s, and maximum injection time of 150 msec. MS3 scans were acquired using SPS of 10 isolation notches, m/z range of 100–1000, 60K resolution, AGC target of 5e4, HCD activation at 55%, and maximum injection time of 250 msec.

Protein Identification and Quantification—Instrument data files (.raw) were converted to mzXML using a modified version of ReadW.exe and MS2 spectra were searched against a database of translated sequences (concatenated in forward and reverse orientation) for all predicted ORFs for *Saccharomyces cerevisiae* (http://www.

yeastgenome.org/download-data; downloaded February 16, 2010) using the Sequest (Ver28) algorithm (14). The added mass of the TMT reagent (229.162932) on lysine residues and peptide N termini, and carbamidomethylation (57.02146) on cysteine were set as fixed modifications. Methionine oxidation (15.99492) was set as a variable modification. A precursor mass tolerance of 10 ppm and 1 Da product ion mass tolerance were used. False positive rates were controlled using the target–decoy approach (15) using the concatenated reversed database. A linear discriminant analysis model was employed to distinguish correct and incorrect peptide identifications based on XCorr, ΔCn, peptide length, and charge state. Peptide hits less than 7 amino acids in length were excluded. After peptides were grouped into proteins, multiplied linear discriminant analysis probabilities were used to score proteins, which were then sorted and filtered to a maximum of 1% false discovery rate. TMT10 reporter ion S/N values in the MS3 scans were used to quantify matching peptides and the sum of reporter ion peptide S/N values for each protein was used in protein quantitation. Unless otherwise noted, relative protein levels are expressed as a percent of the total S/N for all samples. Data sets have been deposited to the PRIDE database and can be accessed using the accession numbers PXD001334 (Fusion Replicate 1), PXD002092 (Fusion Replicate 2), PXD002093 (Fusion Replicate 3), PXD001335 (Elite), and PXD001338 (ΔHap2).

Temporal Profile Matching and Functional Analysis—Triplicate data sets were assessed for significance using the time course package in R Bioconductor, which uses a multivariate empirical Bayes model to rank temporally changing proteins (16). The mb.long function was employed to calculate a Hoteling T^2 statistic and rank proteins according to their temporal abundance changes using a one-dimensional method (where one-sample protein profiles are tested against the null hypothesis that the expected temporal profile = 0). The top 48% (as suggested by the % moderation values calculated by time course) of T^2-ranked proteins (T^2>127) (Fig. 2) were selected for further temporal profiling using a template matching strategy. For template matching, temporal profiles were assumed to match 1 of 6 profiles; induced early, induced late, induced then repressed, repressed early, repressed late, repressed then induced. Template values used for each time point are shown in supplemental Data file S3. Proteins were matched against each temporal profile using the summed Euclidean distance for all time-points. Proteins were then assigned to the template with the minimum summed Euclidean distance. DAVID analysis (http://david.abcc.ncifcrf.gov/summary.jsp) was conducted for each list using all of the identified protein accession numbers as a background, and using only "molecular function" GO terms. YEASTRACT analysis was conducted using the "rank by TF" function and all activating and inhibiting transcription factors were assessed.

Immunoblotting—Overnight cultures of TAP strains were used to inoculate 6 ml of yeast peptone dextrose at an OD600 nm of 0.1 and cultures were grown at 30 °C with shaking (250 RPM). Log-phase samples (4 ml) were harvested at an OD600 nm of 1–1.2, and stationary-phase samples (1 ml) were harvested after 24 h (OD600 nm of 7–8). Cells were centrifuged at 2500 × *g*, washed with water and stored at −80 °C. Lysis was performed in a buffer containing 50 mM Tris, 150 mM NaCl, 0.5% Nonidet P-40 and 1 tablet of Roche Complete Ultra protease inhibitor mixture (Roche, Madison, WI) per 10 ml lysis buffer. Cells were lysed by three cycles of bead beating (45 s per cycle) using a BioSpec Mini-Beadbeater with 1 min rests on ice between cycles. Lysates were cleared by centrifugation at 13,000 × *g* for 5 min. Protein concentrations were determined using a BCA assay (Thermo-Fisher Scientific, Rochford, IL). Extracts were separated by SDS-PAGE, transferred to nitrocellulose membranes, immunoblotted with peroxidase antiperoxidase antibody (1:1000) (Sigma) for 1 h, and developed using chemiluminescence substrate (Perkin-Elmer, Waltham, MA). Membranes were stripped using Restore Western blot Stripping Buffer (Thermo Scientific) and reprobed using actin (MP Biomedicals, Santa Ana, CA) as a loading control.

RESULTS

Comprehensive 10-plex Temporal Profiling of the Diauxic Shift—To capture the full profile of the diauxic shift, we harvested triplicate cultures of yeast (DBY7286; MATa, ura3, GAL2) at 10 time-points over 33 h after inoculation (Fig. 1*A*). Glucose was exhausted from the media after 15 h, and coincided with a decreased growth rate (OD600 nm) (Fig. 1*B*). After cell lysis and proteolytic digestion, peptide samples were labeled using 10-plex TMT reagents (Fig. 1*A*), mixed equally and fractionated by basic pH reversed phase chromatography into 12 fractions. To collect the quantitative data we employed a 3 h LC-MS3 analysis with synchronous precursor selection (SPS)-enabled Orbitrap Fusion mass spectrometer, designed to achieve both a high level of quantitative precision and number of peptide measurements. We assessed gains in peptide measurements because of the advanced instrument by re-analyzing the fractions from replicate 1 with a previous generation Orbitrap Elite mass spectrometer running a 3 h multinotch LC-MS3 method. We observed nearly twice the number of identified peptides on the Fusion (supplemental Fig. S1*A*) resulting in 24 and 14 total quantified peptides per protein using the Fusion and Elite respectively (supplemental Fig. S1*C*). Further, only 221 proteins were quantified by only 1 peptide on the Fusion compared with 443 on the Elite. Similar numbers of identified proteins were observed for analyses on both instruments (supplemental Fig. S1*B*, supplemental Data file S1, S2).

Herein, we refer only to the 3 replicate data sets analyzed using the Orbitrap Fusion (summarized in Fig. 1*C*). These measurements of the dynamics of the yeast proteome resulted in a data set that models protein abundance changes with a combined depth of coverage and temporal resolution not previously achieved in yeast (>4500 proteins, 10 time points). Quantitative protein measurements in the data set overlap highly with previous static yeast data sets of log phase yeast whereby 3974 proteins are quantified in common between our data set and those identified in log phase yeast by Hebert *et al.* (2), and Kulak *et al.* (3) (supplemental Fig. S2). Data from biological replicates were highly correlated (supplemental Fig. S3). Analysis of replicate data using time course revealed that 48% of the proteins (measured in at least two replicates) in the data set were considered moderated. This corresponded to a time course-generated T^2 statistic of 127. The utility of the T^2 statistic is demonstrated in Fig. 2. We observed few changes between early time points, which confirms the precision of the triplicate LC-MS3 analyses. In validation experiments, samples were grown to log and stationary phase using TAP-tagged strains. These experiments were used to validate the induction or repression of several proteins in the data set by immunoblotting. They include proteins for

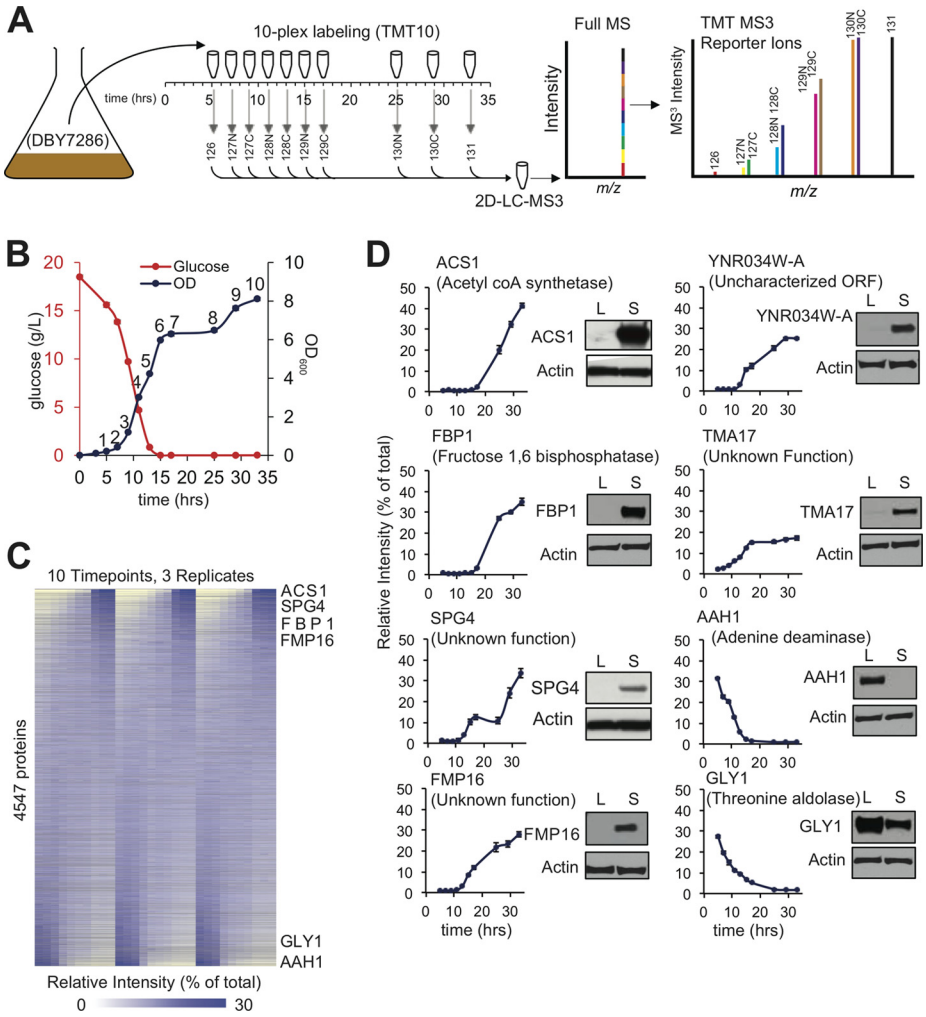

FIG. 1. **Comprehensive and temporal proteomic profiling of the diauxic shift in yeast using TMT10.** *A*, Proteomic sampling and labeling scheme. In triplicate, 10 culture aliquots were acquired over a 33 h time period following inoculation, spanning the logarithmic and stationary phases of growth. Cells were lysed, digested, labeled with TMT10 reagents and combined to a single sample per replicate. Each sample was then separated into 12 fractions by basic-pH reversed phase chromatography and each fraction was analyzed by LC-MS3 using an Orbitrap Fusion mass spectrometer. *B*, Glucose and $OD_{600\ nm}$ throughout the course of the experiment. *C*, Heatmap of relative intensities (% of the total TMT reporter ion signal) for each protein representing abundance changes for 4547 proteins across 10 time-points during the diauxic shift. *D*, Specific examples of temporal protein profile data and validation using immunoblotting of TAP-tagged strains grown to log (L) or stationary phase (S). Error bars represent the standard error of triplicate protein relative intensity measurements.

which a role in the diauxic shift had previously been known (ACS1, FBP1, AAH1, and GLY1) as well as those whose functions are currently unknown (SPG4, FMP16, YNR034W-A, and TMA17) (Fig. 1*D*). Data have been submitted to the PRIDE database (see Methods).

Template matching and functional interpretation—Time-course analysis with 10 time points provided a high level of temporal detail in protein profiles. We thus proposed that we would be able to measure specific temporal patterns of protein induction or repression for the moderated proteins in the data set. A simple template-matching strategy was used whereby protein abundance profiles with T^2 statistics greater than 127 were matched to template profiles. Based around depletion of glucose (at ~15 h) we formed "early-induced," "late-induced," "induced-then-repressed," "early-repressed," "late-repressed," or "repressed-then-induced" template profiles (Fig. 3*A*). The total Euclidean distance was then measured between each protein profile and template profile. Proteins were assigned to the profile with the least total Euclidean distance for all time points (Fig. 3*A*). The corresponding number of matching proteins for each profile were; 899 early-induced proteins, 69 late-induced proteins, 10 induced-then-repressed proteins, 1040 early-repressed proteins, and 72 late-repressed proteins, (Fig. 3*A*, supplemental Data file S3). No proteins matched a template of repressed-then-induced.

To understand the temporal regulation of specific functional groups of proteins during the diauxic shift, we used DAVID functional annotation tool (17) to assign over-represented GO

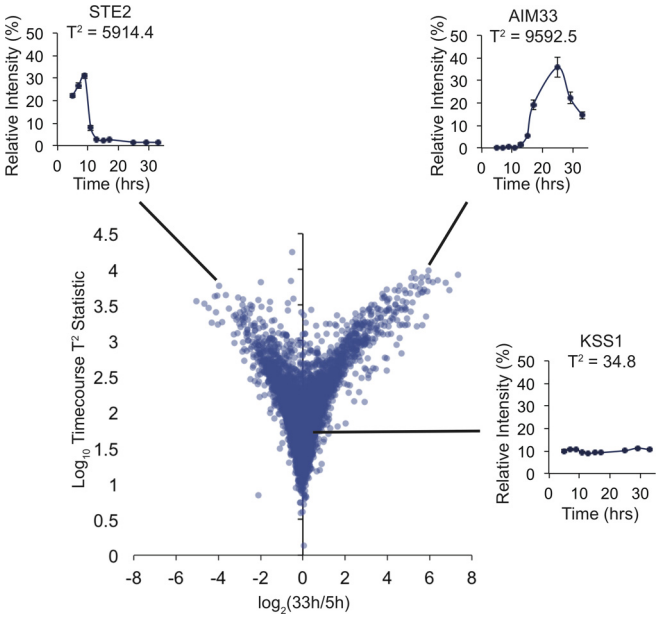

FIG. 2. **Statistical analysis of the triplicate Fusion data sets.** All proteins measured in at least two of the replicate analyses were assigned a T^2 statistic using the *time-course* package in R Bioconductor. Shown are the calculated $\log_{10}$ T^2-statistics plotted against the $\log_2$ values for the 33h/5h time point ratios. Examples are shown demonstrating the utility of the raw *time-course*-generated T^2-statistics in assessing temporal changing proteins.

terms (Benjamini-Hochberg corrected p value < 0.05) to each of the protein profile groupings formed by template matching. We also used the YEASTRACT transcription factor (TF) enrichment tool (18) to determine transcription factors that were over-represented as regulators of expression of proteins within each group. The late-induced proteins were significantly enriched by GO terms "glyoxylate cycle" and "fatty acid oxidation" as well as TF's such as the HAP2,3,4 complex and CAT8. Late-induced temporal regulation of these functions is evidenced by known glyoxylate cycle and fatty acid proteins plotted in Fig. 3*B*. Several proteins of unknown function are also in this late-induced group such as YMR206W (induced by a mean of 163-fold) and YNL195C (induced by a mean of 80-fold) (Fig. 3*B*). In contrast the early-induced proteins were significantly enriched by GO terms "stress response," "glycogen metabolism," "oxidative phosphorylation," and "proteolysis" as well as TF's such as BAS1, MSN2, and MSN4. Early-induced temporal regulation of these functions is evidenced by known stress and oxidative phosphorylation proteins plotted in Fig. 3*C*. Several proteins of unknown function are also in this late-induced group such as ISF1 (induced by a mean of 20-fold), YNR034W-A (induced by a mean of 30-fold), TMA10 (induced by a mean of 80-fold), and TMA17, (induced by a mean of ninefold) (Fig. 3*C*). No GO terms were significantly enriched in the induced-then-repressed group of proteins. However, several proteins of various functions followed this trend including proteins of unknown function including YOR385W (Fig. 3*D*). The early-repressed group of proteins was enriched in "ribosome biogenesis," "amino acid transport," and "RNA-mediated transposition" and TFs such as FHL1 and RAP1. These terms are evidenced by known components of these processes (Fig. 3*E*). In contrast, the late-repressed group of proteins was of various functions and although no GO annotations were enriched in the group, several examples are plotted in Fig. 3*F*.

Comparison to Gene Expression Data—We next compared our data set with the landmark gene expression diauxic shift data set of Derisi *et al.* This data set has served as the most complete model of genomic changes during the diauxic shift in yeast and has been a useful resource in systems biology. As a result of additional time-points we collected after glucose depletion compared with Derisi *et al.*, we capture the induction of many stationary-phase proteins that showed no change in the Derisi *et al.* data set. These are exemplified by GDH3, CIT3, and POX1 (supplemental Fig. S4). For direct comparison, we matched the mean $\log_2$ ratios around the point of glucose exhaustion (15 h in this study, 18 h in Derisi) and compared by heat-map (Fig. 4*A*) and plotting of $\log_2$ ratios against each other (Fig. 4*B*). Although most proteins correlate well, we observed differences between the data sets not attributable to our data set containing additional time-points. For example, the induction of the proteins GAP1, GPH1, and TMA17, and repression of HIP1, CPR4, YNL155W, HXT3, and DOT6 in Fig. 4*C* showed high fold changes in our data prior to glucose exhaustion. These same genes showed either no change or minimal change in the Derisi *et al.* gene expression data. Our protein data set also fully captures protein dynamics during the diauxic shift for 158 proteins (measured in at least two replicates) not measured in the mRNA study and many are induced or repressed significantly at the protein level during the diauxic shift (supplemental Fig. S5*A*, S5*B*). Most of these 158 proteins are small (less than ~100 amino acids long) (supplemental Fig. S6) and thus not considered as true ORFs for the gene expression study. Other larger proteins, are mostly mitochondrial genome-encoded (*e.g.* Q0050), transposable elements (*e.g.* YPL257W-B, YHR214C-B), or plasmid encoded (*e.g.* R0030W) (supplemental Fig. S6), also not considered for the gene expression study.

Temporal Measurements of Isoform-specific Differences—Here, time-course TMT10 with a high number of peptides collected with the Orbitrap Fusion resulted in delineation between important isoforms of metabolic enzymes. Crucially important in the utilization of ethanol in the diauxic shift are alcohol dehydrogenases (ADH1–5). We here benefit from the high number of unique peptides per protein to show the differences in the dynamics between, for example, the ethanol-metabolizing ADH2 isoform and the ethanol-producing ADH1, ADH3, ADH4, and ADH5 isoforms during the diauxic shift (Fig. 5*A*). We also observe differences in temporal dynamics between the aldehyde dehydrogenases (ALD2–6), for which the glucose-repressible ALD2, ALD3, and ALD4 isoforms were induced during the diauxic shift but not the

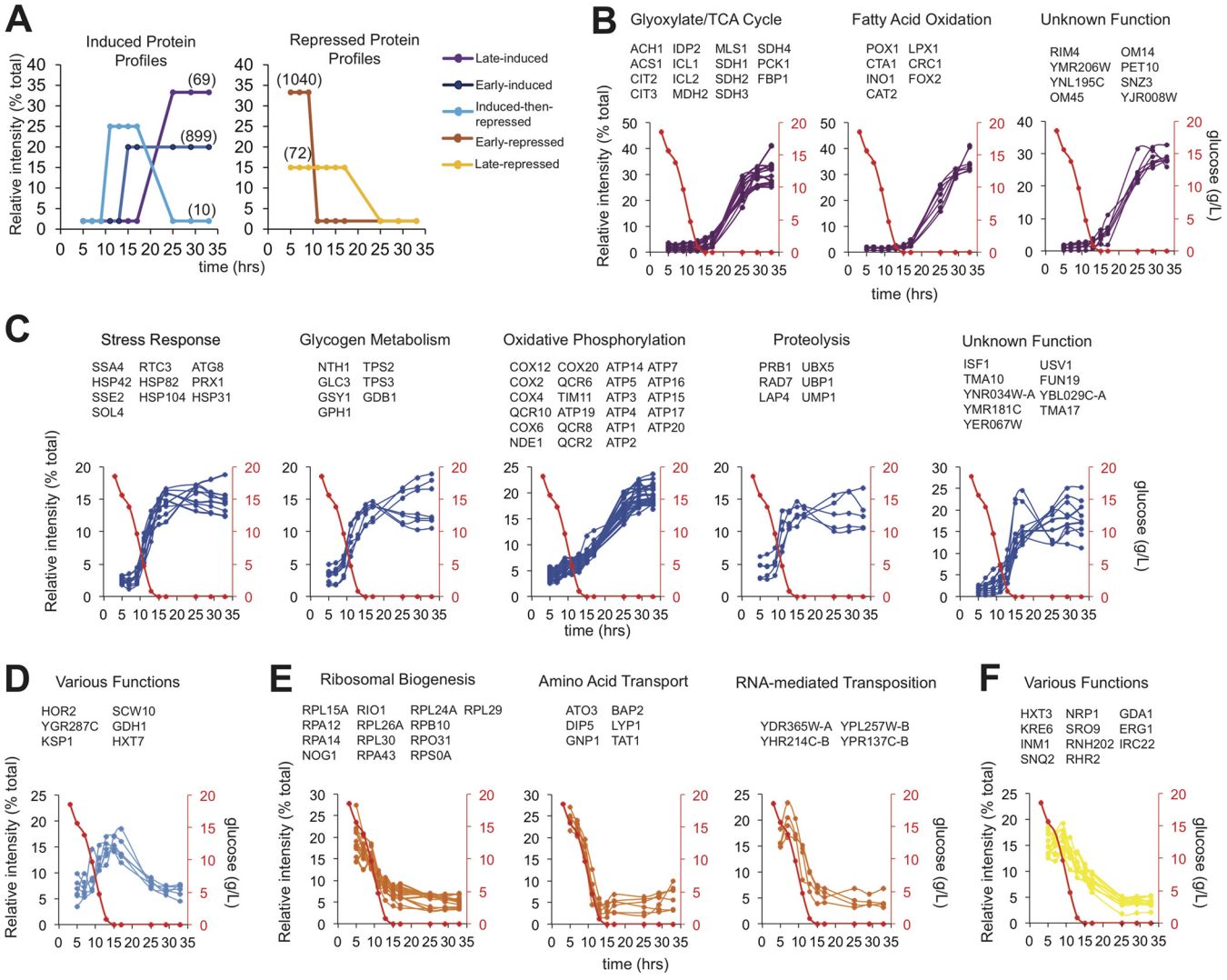

FIG. 3. **Time-course application of TMT10 facilitates comprehensive temporal protein profiling, differentiating between early and late changes in protein abundance during the diauxic shift.** *A*, Proteins from the data set were assessed for significance using the *time-course* package in R, then temporally moderated proteins were matched to specific template protein profiles as shown; early-induced (899 proteins total), late-induced (69 proteins total), induced then repressed (10 proteins total), early-repressed (1040 proteins total), or late-repressed (72 proteins). Matching was based on Euclidean distance between 10-plex TMT protein profiles and the given template. Over-represented GO terms were assigned to the list of proteins matching each template profile using DAVID with a Benjamini Hochberg corrected p value < 0.05. Examples of proteins from over-represented GO terms (if assigned) are shown for *B*, late-induced, *C*, early-induced, *D*, induced then repressed, *E*, early-repressed, and *F*, late-repressed proteins.

K^+/Mg2+-activated ALD5 and ALD6 isoforms (Fig. 5*B*). Glyceraldehyde-3-phosphate dehydrogenase (TDH1–3) and glutamate dehydrogenases (GDH1–3) also display isoform-specific differences in our data set (Fig. 5*C*, 5*D*). Furthermore, although specific amino acid permeases (HIP1, DIP5, TAT1, BAP2, and LYP1) were repressed during the diauxic shift, high affinity general amino acid permeases (GAP1 and AGP1) were induced (supplemental Fig. S7).

10-Plex Dual Time-course to Determine Hap2-dependent Proteins—We next conducted a repeat experiment using a dual time-course 10-plex experimental setup (Fig. 6*A*) to profile both WT and ΔHap2 strains during the diauxic shift. This setup allowed us to both assess reproducibility of our original 10-plex data set and define a putative list of Hap2-regulated proteins. We chose Hap2 because it plays a role in regulating many proteins during the switch to respiratory metabolism during the diauxic shift but such regulation has not been fully described. Also, many of the strongly induced proteins in our initial 10-plex TMT data set are proposed to be regulated by the Hap2,3,4 transcription factor complex. We harvested WT or ΔHap2 yeast over 24 h after inoculation, collecting five time-points for each strain (Fig. 6*A*). We observed no difference between the growth (OD600 nm) or media glucose concentrations between WT and ΔHap2 cells (supplemental Fig.

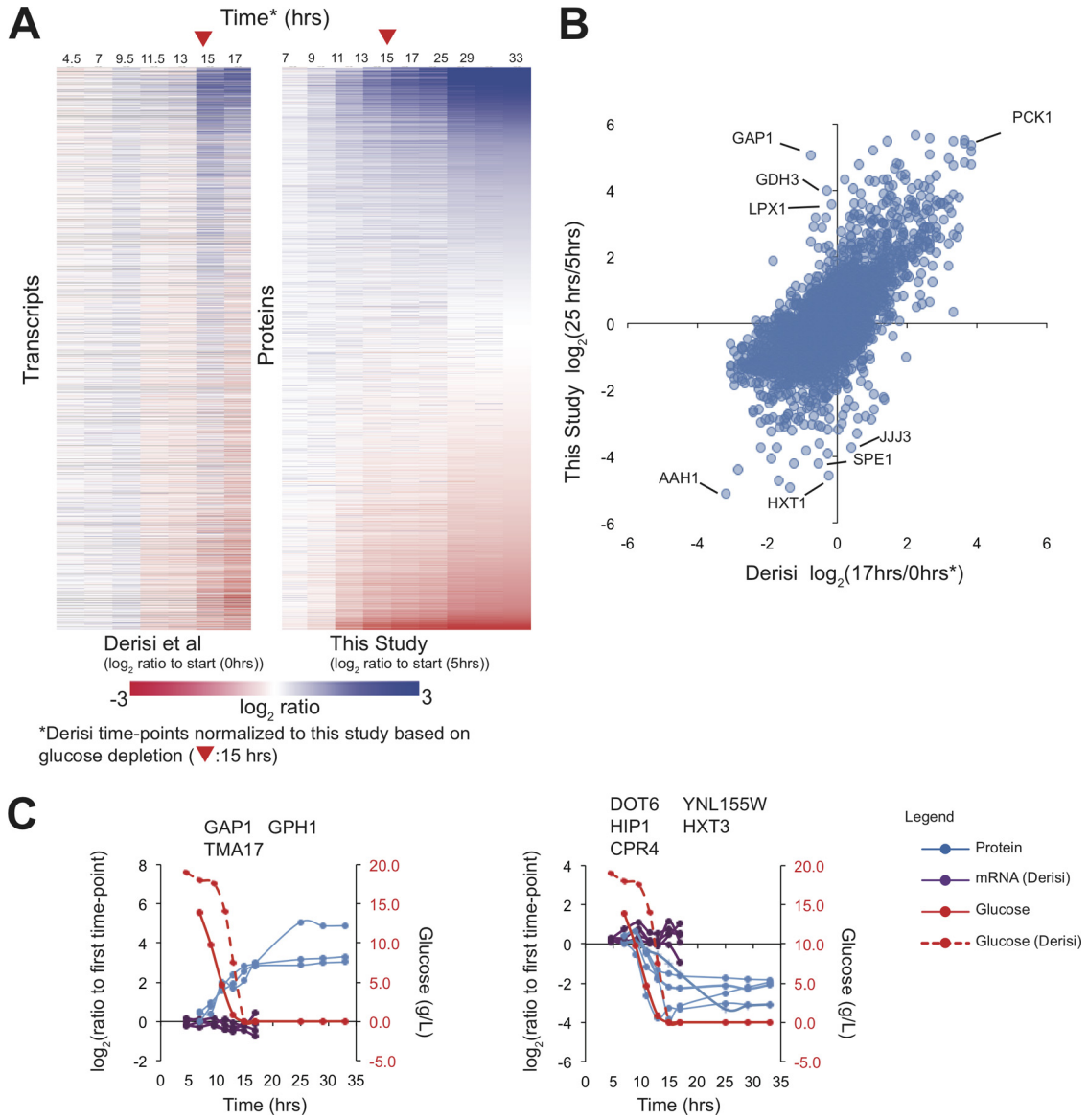

FIG. 4. **Correlation of the time-course TMT10 data set with mRNA data from Derisi *et al.*** *A*, Aligned heatmaps of time-course profiles between the two studies. To directly compare the two studies, data are expressed as $\log_2$ ratios to the earliest time point (proteins shown appear in all 3 replicate TMT10 analyses). *B*, The latest time-points are compared with the earliest time-points for the $\log_2$ ratios in both studies. Genes or proteins in the top-left and bottom-right quadrants differ between this study and Derisi *et al.* *C*, Examples of several proteins induced or repressed in this study (at the protein level) but not in the data set of Derisi *et al.* (mRNA level).

S8). Cells were lysed, digested, labeled with 10-plex TMT reagents, separated into 12 fractions using basic-pH reversed phase chromatography and analyzed by an LC-MS3 method (Fig. 6*A*). A side-by-side comparison of protein profiles from our first and second 10-plex experiments, which were performed on two different yeast strains (DBY7286 and BY4742) confirms a high degree of reproducibility for protein diauxic shift responses between these two strains (Fig. 6*B*). We also confirm their correlation by comparing $\log_2$ ratios of representative time-points between the first (25 h/5 h ratio) and the second (24 h/4 h ratio) experiments (WT-only) (supplemental Fig. S9). These data demonstrate the repeatability of the diauxic shift between these two strains. Hap2-dependent proteins were determined from differences between protein profiles of the WT and ΔHap2 strains. We observed few differences between WT and ΔHap2 strains in log phase before glucose was exhausted (supplemental Fig. S10). However, in stationary phase (24 h) (supplemental Fig. S10) we observed 63 proteins with WT-ΔHap2 differences greater than 10 (mean fold difference of 3.8). These proteins we considered to have the strongest Hap2-dependence (supplemental Data file S4). Analysis of

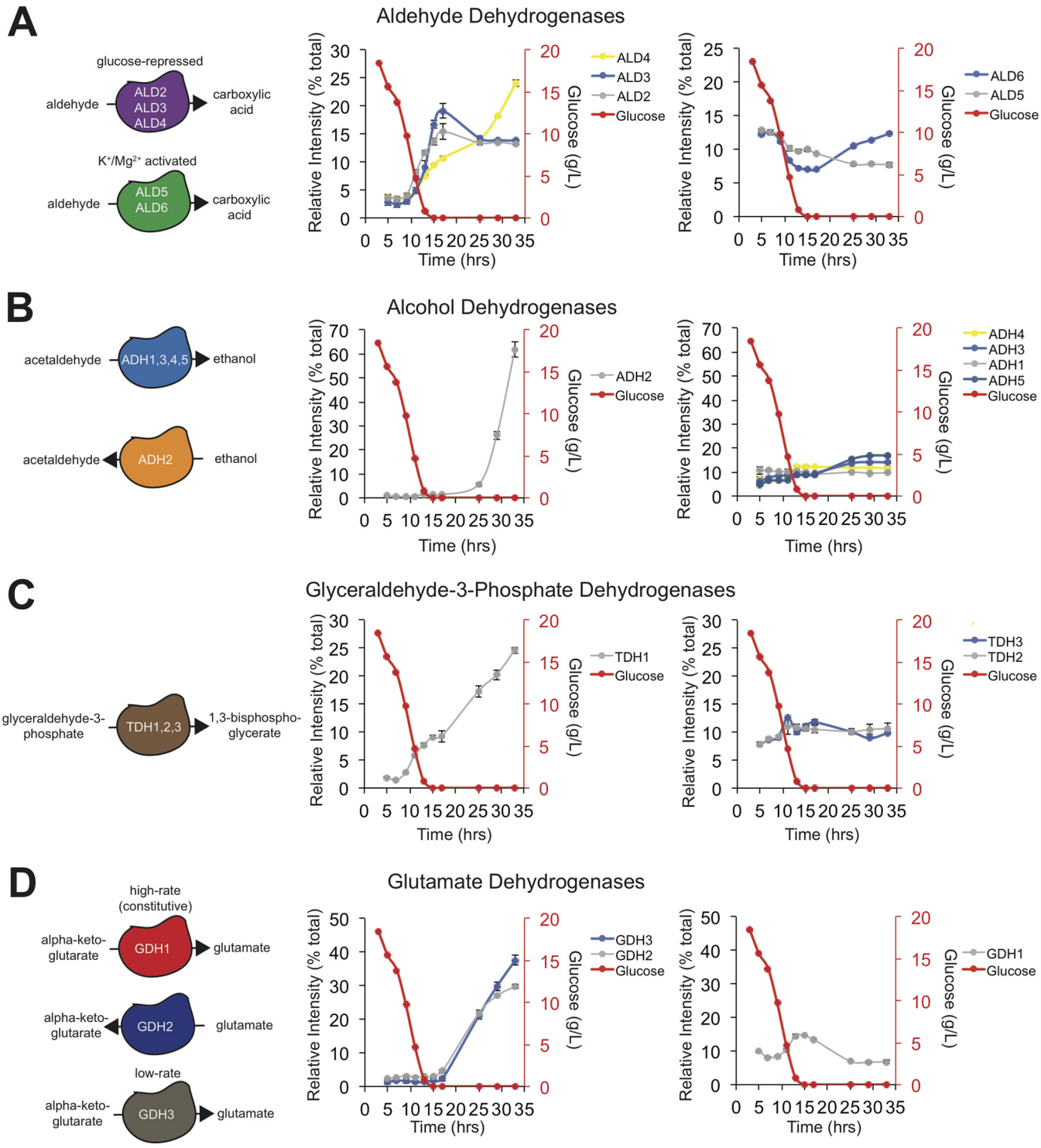

FIG. 5. **Differences in the induction of specific isoforms of various metabolically important proteins during the diauxic shift;** *A*, Aldehyde dehydrogenases, *B*, Alcohol dehydrogenases, *C*, Glyceraldehyde-3-phosphate dehydrogenases, and *D*, Glutamate dehydrogenases. Error bars represent the standard error of triplicate protein relative intensity measurements.

these 63 proteins using DAVID functional annotation tool (Benjamini-Hochberg corrected p value < 0.05) revealed enrichment of the GO terms glyoxylate metabolism and oxidative phosphorylation. These annotations are evidenced by known glyoxylate metabolism and oxidative phosphorylation proteins shown in Fig. 6*C*. Among these proteins we also observed Hap2-dependence for proteins contributing to the glyoxylate pathway via carnitine metabolism (CAT2 and

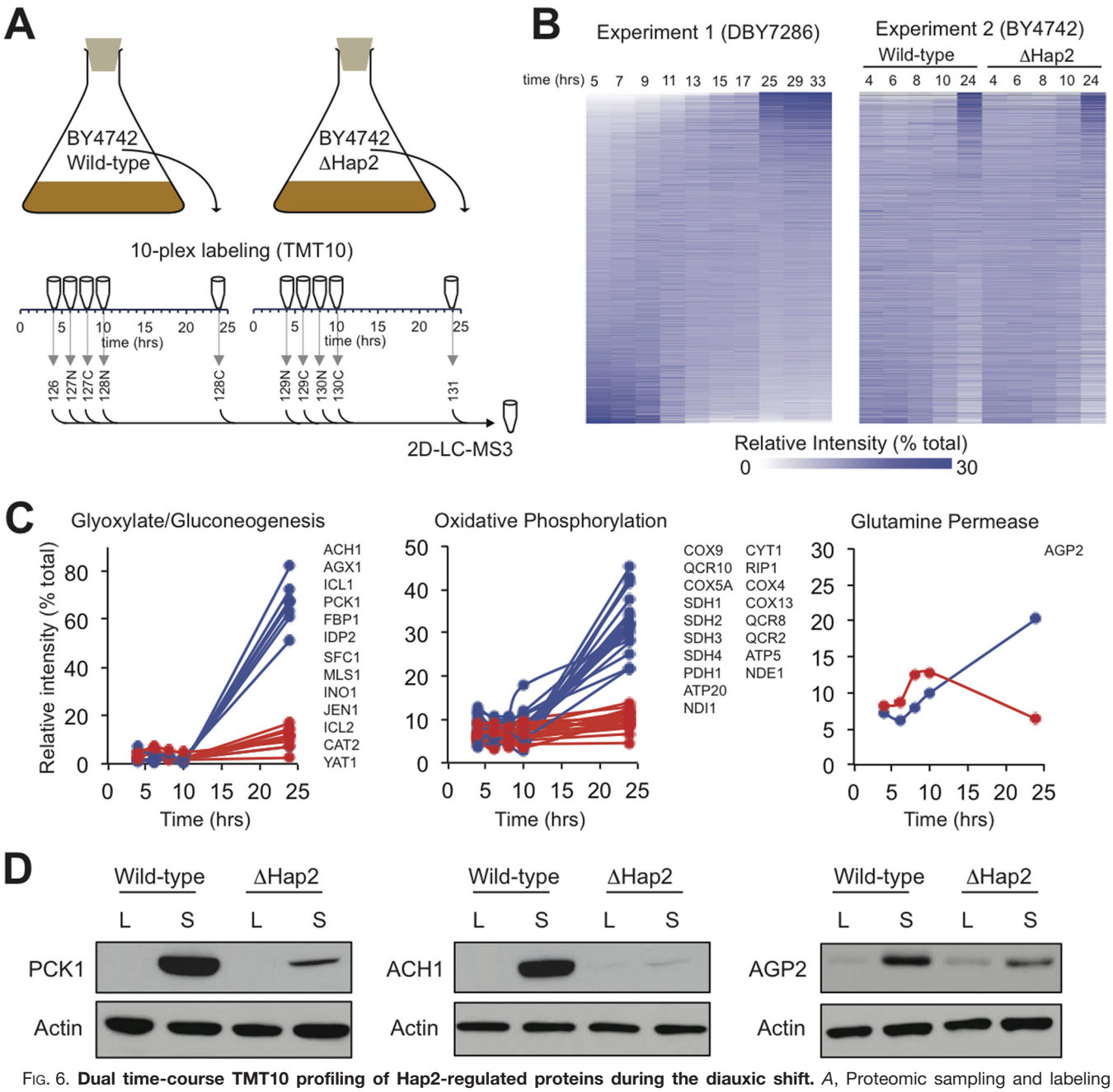

FIG. 6. **Dual time-course TMT10 profiling of Hap2-regulated proteins during the diauxic shift.** *A*, Proteomic sampling and labeling scheme. Five aliquots from BY4742 WT and ΔHap2 strains were acquired over a 24 h time period following inoculation, spanning the logarithmic and stationary phases of growth. Cells were lysed, digested, labeled with 10-plex reagents and combined to a single sample. The sample was then separated into 12 fractions by basic-pH reversed phase chromatography and each fraction was analyzed by LC-MS3. *B*, Reproducibility between experiments represented by aligned heatmaps of relative intensities (% of the total for each protein) for the initial 10-plex time-course and the 10-plex dual time-course. *C*, Proteins with relative intensity differences between WT (Blue) and ΔHap2 (Red) during the diauxic shift. *D*, Validation of PCK1, ACH1, and AGP2 dependence on Hap2. Each protein was TAP-tagged in the ΔHap2 strain and measured by immunoblot in a separate experiment in either log (L) or stationary (S) phase.

YAT1). Interestingly, we also observe Hap2-dependence for the glutamine permease, AGP2 (Fig. 6C), which acts further upstream of carnitine metabolism. For confirmation of some observed Hap2-dependent proteins in the data set, we first TAP-tagged several in the ΔHap2 background. Then, in repeat experiments, we grew these TAP strains to log and stationary phase. By TAP immunoblotting we confirm Hap2-dependence for proteins with known Hap2-regulated functions (PCK1 and ACH1) and for AGP2 (Fig. 6*D*).

Surprisingly, we observed 53 proteins that had WT-ΔHap2 differences less than −10 (mean fold difference of 2.2) (supplemental Data file S4). These proteins were considered either

negatively regulated by Hap2 under WT conditions or induced to compensate stress caused by the reduction in abundance of many of the Hap2-regulated proteins. Functional analysis of these 53 proteins revealed enrichment of GO terms related for heat stress. Data have been submitted to the PRIDE database (see methods).

DISCUSSION

Protein abundance in yeast is dynamic and a greater understanding of temporal protein dynamics during utilization of different substrates provides insight to protein function. Proteome dynamics during the diauxic shift are particularly important because they serve as a basic model for fermentative *versus* respiratory metabolism underlying cancer cell proliferation. We here use 10-plex TMT to achieve comprehensive proteome analysis (4547 proteins) over 10 time-points of the diauxic shift thus resulting in more than 45,000 protein measurements in a single experiment. The data set is unique in that it fully captures the diauxic shift over an extended time-course with the temporal resolution needed to distinguish expression patterns at a comprehensive level. We were thus able to determine global patterns of late- *versus* early-induction of proteins in the diauxic shift (Fig. 3). We have ensured a high level of accuracy by collecting the data in biological triplicate and performing MS3 reporter ion quantitation using SPS on the Orbitrap Fusion mass spectrometer. This has allowed quantitation of more total peptides per protein (24 on average (single replicate) than by analysis with a previous generation, Orbitrap Elite, mass spectrometer (14 on average) and more than previous yeast duplex quantitative studies of 11 (19) and 15 (20) (on average).

Although, it was the subject of a landmark study of the first comprehensive microarray analysis to understand gene regulation in eukaryotes (4), proteomic approaches toward the diauxic shift have suffered from either low proteomic depth of targeted mass spectrometry or the low sample throughput of shotgun approaches. For example, using multiple reaction monitoring (MRM) to profile the diauxic shift has offered temporal coverage of central carbon metabolism, but at a depth of less than 100 proteins. Although not comprehensive, a shotgun approach employing four-plex labeling by amine-reactive neutron-encoded labels has allowed more proteins to be quantified (1543) but with lower coverage of carbon metabolism and few time-points to delineate temporal patterns (21). More recently, six-plex TMT achieving comprehensive levels of protein quantifications of either log phase or stationary phase (6). However, the study did not aim to capture the temporal transition between the two states as we have done here so many diauxic shift-regulated proteins were not shown to change in abundance. For example, in the six-plex study, proteins such as FBP1, a well-known stationary phase-induced gluconeogenesis protein, did not change within log or stationary phase, but a mean of 76.2-fold induction was captured in our data set.

The previous most comprehensive and temporal "omics" capture of the diauxic shift is thus the gene expression data set of Derisi *et al.* (Fig. 4), which allowed us to assess further the accuracy of our proteomic data set. The same yeast strain (DBY7286) was used in both studies. Many of the temporal patterns we observe here are consistent with the seven time point gene expression data set of Derisi *et al.*, in which the induction of stress and oxidative phosphorylation proteins precedes glucose depletion but induction of glyoxylate proteins occurs after glucose depletion (Fig. 3). This strategy is important in yeast survival because stress-related proteins must be induced to handle accompanying increases in oxidative stress during the respiratory transition. Indeed, in Fig. 3, stress response proteins slightly precede a more gradual induction of oxidative phosphorylation proteins. Once glucose is depleted, cells then induce proteins to fuel respiration through glyoxylate metabolism (using ethanol) and fatty acid oxidation, also evident in Fig. 3. The over-represented transcription factors we observed for each pattern of induction are consistent with their roles in stress (MSN2, MSN4, and HSF1 in early-induced proteins) and glyoxylate cycle function (Hap2,3,4, and CAT8 in late-induced proteins) (22, 23). The temporal groupings also provide insight to the regulation of proteins of unknown function. For example, YNR034W-A (Fig. 1*D*) has previously been shown to be regulated by MSN2/MSN4 (24) and thus may play a role in cell stress. An interesting group of proteins that emerged from our temporal analysis are those induced before but repressed after glucose depletion (Fig. 3), the functions of which are varied or unknown but likely important in nutrient responses. For example, KSP1, which was induced-then-repressed is a serine/threonine kinase involved in TOR signaling (25).

The repression of ribosomal proteins we observed is consistent with the study of Derisi *et al.* and other studies, whereby the energy-intensive process of ribosomal biogenesis is repressed under various stress conditions. By virtue of the high temporal resolution of our data, we were able to observe a decrease in ribosomal protein abundance prior to glucose depletion, rather than after as in the gene expression data set of Derisi *et al.* This suggests a role for either degradation or decreased translation of ribosomal proteins prior to their repression at the transcript level, or involvement of yet-unknown regulatory pathways. Although several of these proteins have previously been shown to be decreased translationally upon glucose depletion (26), their repression prior to glucose depletion suggests they are regulated by other factors such as oxidative stress. Notably, oxidative stress proteins are also induced at this time (Fig. 3). The over-represented transcription factors in the repressed protein group is consistent with their regulation by ribosome-regulating transcription factors FHL1 and RAP1, which are highly active only during growth on glucose (27).

Apart from some of the more characterized diauxic-shift related protein changes already mentioned by others such as

the glyoxylate pathway and gluconeogenesis, many more proteins of unknown functions are induced or repressed in our data set. Many were not previously profiled during log to stationary phase transition. The 158 proteins not included in the Derisi *et al.* data set were mainly not previously measured because they are small (*e.g.* SIP18), mitochondria-encoded (*e.g.* Q0050), or plasmid-encoded (*e.g.* YPL257W-B). The diauxic shift data for these proteins is thus novel, and many of them were shown to be highly induced or repressed (supplemental Fig. S5). Included in this group is the aforementioned, early-induced, YNR034W-A. Many differences we observed resulted from the 10-plex nature of the experiment that allowed data collection over more time-points after glucose depletion (*e.g.* GDH3 and POX1, supplemental Fig. S4). These examples illustrate the benefit of fully capturing the diauxic transition. Other diauxic shift-regulated proteins unique to our data that were induced before glucose exhaustion are consistent with other literature. For example GAP1 and GPH1 gene expression (Fig. 4*C*) have been shown to be induced during various stress conditions including glucose deprivation (5, 28).

Whereas the Derisi *et al.* data set did not distinguish between several important isoforms of, for example, aldehyde dehydrogenases because of cross-hybridization of similar sequences, our data set does (Fig. 5). Such specificity is important in yeast biology because the glucose-repressible ADH2 isoform catalyzes the formation of acetaldehyde from ethanol, whereas the others catalyze the reverse reaction during fermentative metabolism (29). The isoform-specific expression of aldehyde dehydrogenases in our data set is also consistent with known behavior of these proteins during the diauxic shift (5). The ability to globally measure differences in groups of functionally similar proteins highlights the comprehensiveness of our data set. For example, we profiled most of the known amino acid permeases, and show high induction of general amino acid permeases (GAP1 and AGP1), consistent with previous studies (30), but a clear repression of specific amino acid permeases (supplemental Fig. S7).

Confirming the accuracy of our data set, our results were reproducible in a second experiment with a different WT yeast strain (Fig. 6) in the dual time-course experiment. In yeast, global proteomic analysis in deletion strains has been performed in duplex but many yeast pathways are only regulated dynamically. For example, many transcription factors are only activated during the transition to stationary phase and thus require temporal quantitation. Such is the case for the Hap2,3,4 TF complex (31), which is predicted to regulate many of the proteins we observed to be induced during the diauxic shift. Hap2 is a crucial component of this complex (1). Our global, dual time-course data set comparing WT and ΔHap2 strains demonstrates the benefit of 10-plex TMT to facilitate the analysis of temporally dependent regulatory proteins. High similarity between the temporal protein changes of WT and ΔHap2 strains (Fig. 6*B*) provided confidence in our ability to select Hap2-regulated proteins. Moreover, the differences we detect between the WT and ΔHap2 strains almost exclusively occur after the diauxic shift (at the 24 h time point) highlighting the role of Hap2 in the transition to respiratory growth. Our observation that many glyoxylate cycle, gluconeogenesis, and oxidative phosphorylation proteins are dependent upon Hap2 during the diauxic shift is consistent with the predicted regulation of the these processes by the Hap2,3,4 complex. These observations are also consistent with a previous gene expression analysis of Hap2-induced genes grown on galactose (32), which simulates substrate utilization during stationary phase and activates similar regulatory networks. Previous reports have not, however, made a relationship between Hap2 and the induction of carnitine metabolism proteins. Specifically of interest from our data was regulation of carnitine acetyl tranferases, CAT2 and YAT1, as well as the carnitine transport protein AGP2 (33). We confirm AGP2 as a Hap2-dependent protein during stationary phase (Fig. 6*D*). Further studies are needed to better understand the role of Hap2 in regulating carnitine metabolism. Carnitine metabolism regulation by Hap2, although not understood, is consistent with other Hap2-regulated proteins because carnitine provides acetyl CoA to the glyoxylate cycle. Negative regulation of stress related proteins (*e.g.* HSP12, SOL4) has also not previously been linked to Hap2 but should be further explored. Although we observed no reduction in growth or glucose consumption in ΔHap2 cells, growth differences may not be expected until several hours beyond the time-course of this experiment. Besides determining Hap2-dependent proteins, we propose that similar 10-plex TMT dual time-course experiments (*e.g.* WT *versus* deletion strains) have the potential to help understand other regulatory networks important during temporal shift.

To conclude, we utilized 10-plex TMT and the SPS-MS3 method to conduct a comprehensive mapping of protein abundance dynamics during the diauxic shift in yeast. Our data set fully captures time-resolved expression measurements such that proteins of similar temporal expression profiles could be grouped, representing distinct functions. We further demonstrate a dual time-course TMT10 approach, detailing proteins dependent on the respiratory transcription factor, Hap2, and revealing a connection between Hap2 and carnitine metabolism. The high level of both analysis depth and temporal resolution make these data a valuable resource to the yeast community. Further, as the most temporally resolved shotgun proteomics study to date (10 time-points) these data represent a benchmark in measuring temporal protein dynamics to understand protein regulation.

§ To whom correspondence should be addressed: Department of Cell Biology, Building C, Room 516, Harvard Medical School, 240 Longwood Avenue, Boston, MA 02115. Tel.: 617-432–3155; Fax: 617-432–1144; E-mail: sgygi@hms.harvard.edu.

[S] This article contains supplemental Figs. S1 to S10 and Data files S1 to S4.

REFERENCES

1. Botstein, D., and Fink, G. R. (2011) Yeast: an experimental organism for 21st century biology. *Genetics* **189,** 695–704
2. Hebert, A. S., Richards, A. L., Bailey, D. J., Ulbrich, A., Coughlin, E. E., Westphall, M. S., and Coon, J. J. (2014) The one hour yeast proteome. *Mol. Cell. Proteomics* **13,** 339–347
3. Kulak, N. A., Pichler, G., Paron, I., Nagaraj, N., and Mann, M. (2014) Minimal, encapsulated proteomic-sample processing applied to copy-number estimation in eukaryotic cells. *Nat. Methods* **11,** 319–324
4. DeRisi, J. L., Iyer, V. R., and Brown, P. O. (1997) Exploring the metabolic and genetic control of gene expression on a genomic scale. *Science* **278,** 680–686
5. Brauer, M. J., Saldanha, A. J., Dolinski, K., and Botstein, D. (2005) Homeostatic adjustment and metabolic remodeling in glucose-limited yeast cultures. *Mol. Biol. Cell* **16,** 2503–2517
6. Slavov, N., Budnik, B. A., Schwab, D., Airoldi, E. M., and van Oudenaarden, A. (2014) Constant growth rate can be supported by decreasing energy flux and increasing aerobic glycolysis. *Cell Reports* **7,** 705–714
7. McAlister, G. C., Huttlin, E. L., Haas, W., Ting, L., Jedrychowski, M. P., Rogers, J. C., Kuhn, K., Pike, I., Grothe, R. A., Blethrow, J. D., and Gygi, S.P. (2012) Increasing the multiplexing capacity of TMTs using reporter ion isotopologues with isobaric masses. *Anal. Chem.* **84,** 7469–7478
8. Thompson, A., Schafer, J., Kuhn, K., Kienle, S., Schwarz, J., Schmidt, G., Neumann, T., Johnstone, R., Mohammed, A. K., and Hamon, C. (2003) Tandem mass tags: a novel quantification strategy for comparative analysis of complex protein mixtures by MS/MS. *Anal. Chem.* **75,** 1895–1904
9. Ting, L., Rad, R., Gygi, S. P., and Haas, W. (2011) MS3 eliminates ratio distortion in isobaric multiplexed quantitative proteomics. *Nat. Methods* **8,** 937–940
10. McAlister, G. C., Nusinow, D. P., Jedrychowski, M. P., Wuhr, M., Huttlin, E. L., Erickson, B. K., Rad, R., Haas, W., and Gygi, S. P. (2014) MultiNotch MS3 enables accurate, sensitive, and multiplexed detection of differential expression across cancer cell line proteomes. *Anal. Chem.* **86**. 7150–7158
11. Senko, M. W., Remes, P. M., Canterbury, J. D., Mathur, R., Song, Q., Eliuk, S. M., Mullen, C., Earley, L., Hardman, M., Blethrow, J. D. Bui, H., Specht, A., Lange, O., Denisov, E., Makarov, A., Horning, S., and Zabrouskov, V. (2013) Novel parallelized quadrupole/linear ion trap/orbitrap tribrid mass spectrometer improving proteome coverage and peptide identification rates. *Anal. Chem.* **85,** 11710–11714
12. Ghaemmaghami, S., Huh, W. K., Bower, K., Howson, R. W., Belle, A., Dephoure, N., O'Shea, E. K., and Weissman, J. S. (2003) Global analysis of protein expression in yeast. *Nature* **425,** 737–741
13. Rappsilber, J., Ishihama, Y., and Mann, M. (2003) Stop and go extraction tips for matrix-assisted laser desorption/ionization, nanoelectrospray, and LC/MS sample pretreatment in proteomics. *Anal. Chem.* **75,** 663–670
14. Eng, J. K., McCormack, A. L., and Yates, J. R. (1994) An approach to correlate tandem mass spectral data of peptides with amino acid sequences in a protein database. *J. Am. Soc. Mass Spectrom.* **5,** 976–989
15. Elias, J. E., and Gygi, S. P. (2007) Target-decoy search strategy for increased confidence in large-scale protein identifications by mass spectrometry. *Nat. Methods* **4,** 207–214
16. Tai, Y.C. (2007) timecourse: Statistical analysis for developmental microarray time course data. R package version 1.38.0 http://www.bioconductor.org
17. Huang, da, W., Sherman, B. T., and Lempicki, R. A. (2008) Systematic and integrative analysis of large gene lists using DAVID bioinformatics resources. *Nat. Protoc.* **4,** 44–57
18. Teixeira, M. C., Monteiro, P., Jain, P., Tenreiro, S., Fernandes, A. R., Mira, N. P., Alenquer, M., Freitas, A. T., Oliveira, A. L., and Sa-Correia, I. (2006) The YEASTRACT database: a tool for the analysis of transcription regulatory associations in Saccharomyces cerevisiae. *Nucleic Acids Res.* **34,** D446-D451
19. de Godoy, L. M., Olsen, J. V., Cox, J., Nielsen, M. L., Hubner, N. C., Frohlich, F., Walther, T. C., and Mann, M. (2008) Comprehensive mass-spectrometry-based proteome quantification of haploid versus diploid yeast. *Nature* **455,** 1251–1254
20. Wu, R., Dephoure, N., Haas, W., Huttlin, E. L., Zhai, B., Sowa, M. E., and Gygi, S. P. (2011) Correct interpretation of comprehensive phosphorylation dynamics requires normalization by protein expression changes. *Mol. Cell. Proteomics* **10,** M111. 009654
21. Hebert, A. S., Merrill, A. E., Stefely, J. A., Bailey, D. J., Wenger, C. D., Westphall, M. S., Pagliarini, D. J., and Coon, J. J. (2013) Amine-reactive neutron-encoded labels for highly plexed proteomic quantitation. *Mol. Cell. Proteomics* **12,** 3360–3369
22. Boy-Marcotte, E., Perrot, M., Bussereau, F., Boucherie, H., and Jacquet, M. (1998) Msn2p and Msn4p control a large number of genes induced at the diauxic transition which are repressed by cyclic AMP in saccharomyces cerevisiae. *J. Bacteriol.* **180,** 1044–1052
23. Boy-Marcotte, E., Lagniel, G., Perrot, M., Bussereau, F., Boudsocq, A., Jacquet, M., and Labarre, J. (1999) The heat shock response in yeast: differential regulations and contributions of the Msn2p/Msn4p and Hsf1p regulons. *Mol. Microbiol.* **33,** 274–283
24. Lai, L. C., Kosorukoff, A. L., Burke, P. V., and Kwast, K. E. (2005) Dynamical remodeling of the transcriptome during short-term anaerobiosis in Saccharomyces cerevisiae: differential response and role of Msn2 and/or Msn4 and other factors in galactose and glucose media. *Mol. Cell. Biol.* **25,** 4075–4091
25. Umekawa, M., and Klionsky, D. J. (2012) Ksp1 kinase regulates autophagy via the target of rapamycin complex 1 (TORC1) pathway. *J. Biol. Chem.* **287,** 16300–16310
26. Castelli, L. M., Lui, J., Campbell, S. G., Rowe, W., Zeef, L. A., Holmes, L. E., Hoyle, N. P., Bone, J., Selley, J. N., Sims, P. F., Ashe, M. P. (2011) Glucose depletion inhibits translation inititaion via eiF4A loss and subsequent 48S preinitiation complex accumulation, while the pentose phosphate pathway is coordinately up-regulated. *Mol. Biol. Cell* **22,** 3379–3393
27. Wade, J. T., Hall, D. B., and Struhl, K. (2004) The transcription factor Ifh1 is a key regulator of yeast ribosomal protein genes. *Nature* **432,** 1054–1058
28. Gasch, A. P., Spellman, P. T., Kao, C. M., Carmel-Harel, O., Eisen, M. B., Storz, G., Botstein, D., and Brown, P. O. (2000) Genomic expression programs in the response of yeast cells to environmental changes. *Mol. Biol. Cell* **11,** 4241–4257
29. Russell, D. W., Smith, M., Williamson, V. M., and Young, E. T. (1983) Nucleotide sequence of the yeast alcohol dehydrogenase II gene. *J. Biol. Chem.* **258,** 2674–2682
30. Regenberg, B., During-Olsen, L., Kielland-Brandt, M. C., and Holmberg, S. (1999) Substrate specificity and gene expression of the amino-acid permeases in Saccharomyces cerevisiae. *Current Genet.* **36,** 317–328
31. Forsburg, S. L., and Guarente, L. (1989) Communication between mitochondria and the nucleus in regulation of cytochrome genes in the yeast Saccharomyces cerevisiae. *Ann. Rev. Cell Biol.* **5,** 153–180
32. Buschlen, S., Amillet, J. Ä., Guiard, B., Fournier, A., Marcireau, C., and Bolotin-Fukuhara, M. (2003) The S. cerevisiae HAP complex, a key regulator of mitochondrial function, coordinates nuclear and mitochondrial gene expression. *Comparative Func. Genomics* **4,** 37–46
33. Lee, J., Lee, B., Shin, D., Kwak, S. S., Bahk, J. D., Lim, C. O., and Yun, D. J. (2002) Carnitine uptake by AGP2 in yeast Saccharomyces cerevisiae is dependent on Hog1 MAP kinase pathway. *Mol. Cells* **13,** 407–412